PHILOSOPHICAL TRANSACTIONS OF THE ROYAL SOCIETY A MATHEMATICAL, PHYSICAL & ENGINEERING SCIENCES

Ions Trapped below the Surface of Superfluid Helium. I. The Observation of Plasma Resonances, and the Measurement of Effective Masses and Ionic Mobilities

C. F. Barenghi, C. J. Mellor, J. Meredith, C. M. Muirhead, P. K. H. Sommerfeld and W. F. Vinen

Phil. Trans. R. Soc. Lond. A 1991 **334**, 139-172
doi: 10.1098/rsta.1991.0005

Ions trapped below the surface of superfluid helium. I. The observation of plasma resonances, and the measurement of effective masses and ionic mobilities

By C. F. Barenghi†, C. J. Mellor‡, J. Meredith, C. M. Muirhead, P. K. H. Sommerfeld and W. F. Vinen

Department of Physics, University of Birmingham, Birmingham B15 2TT, U.K.

Contents

The results are reported of experiments on two-dimensional pools of positive and negative ions trapped below the surface of superfluid ^{4}He. The results of detailed computations on the static characteristics of an ion pool are presented, from which it is possible to deduce the size of the pool from the known potentials applied to the surrounding electrodes and the measured total charge in the pool. At the higher temperatures, between 1 K and about 300 mK, the ionic mobility can be obtained from measurements of the non-resonant response of the ions in the pool with a capacitance–conductance bridge connected to a pair of the surrounding electrodes; the theory underlying this technique is described in detail, and experimental results are presented. At lower temperatures sharp plasma resonances can be excited, and detailed studies of these resonances have been made in the temperature range from

† Present address: School of Mathematics, The University, Newcastle-upon-Tyne NE1 7RU, U.K.
‡ Present address: Department of Physics, University of Nottingham, Nottingham NG7 2RD, U.K.

Phil. Trans. R. Soc. Lond. A (1991), **334**, 139–172
Printed in Great Britain

25 mK to 130 mK for negative ions and from 15 mK to 450 mK for positive ions. Ionic effective masses have been deduced from the observed resonant frequencies, but the resulting values are in some respects unreliable for reasons that are explained. Ionic mobilities have been deduced from the observed damping of the plasma resonances; they are compared with the results of earlier experiments at higher temperatures, but the comparison with theory will be presented in a separate paper. The ion pools have been cooled on many occasions below the temperature at which there is a transition to a Wigner crystal, but no corresponding change has been observed in the behaviour of the mobility or of the plasma resonances.

1. Introduction

Charged particles can be trapped either above or below the free surface of superfluid helium. An electron above the surface is attracted to the helium by its image charge or by an external electric field, but penetration of the helium is opposed by a potential barrier of about 1 eV. The electron is free to move over the surface, but at the temperatures of superfluid helium it is trapped in the vertical direction in a single quantum state. An assembly of such electrons forms a two-dimensional system that is practically ideal in its behaviour, and many interesting and important experiments on this system have been reported (see, for example, Dahm & Vinen 1987). Charged particles can also be trapped below the surface of superfluid helium. In this case the image repels the particle from the surface, but the addition of a uniform external electric field, E_0, forcing the particle upwards towards the surface causes the particle to experience a net potential given as a function of depth, z, by

$$V(z) = eE_0 z + (\epsilon - 1)\, e^2/16\pi\epsilon_0\, \epsilon(\epsilon+1)\, z, \tag{1.1}$$

where ϵ is the dielectric constant of the liquid, and it is assumed that the density of the vapour above the liquid is negligible. Charged particles can therefore be trapped at or near the minimum in the potential (1.1), which is at a depth given by

$$z_0^2 = (\epsilon - 1)\, e/16\pi\epsilon_0\, \epsilon(\epsilon+1)\, E_0. \tag{1.2}$$

For a field E_0 of about 5 kV m^{-1} the depth z_0 is about 43 nm.

Two types of charged particle can be produced rather easily in liquid helium by, for example, applying a suitable potential to a field emission or field ionization tip immersed in the liquid. The so-called *positive ion* consists probably of a He_2^+ ion embedded in a tiny sphere of solid helium, formed around it as a result of enhancement of the local pressure by electrostriction (Atkins 1959); the radius of the sphere is about 0.55 nm when the helium far from the ion is at a low pressure. The *negative ion* is formed from an electron. Since, as we have mentioned, a large potential barrier opposes penetration of the electron into the liquid, the electron repels the helium atoms in its neighbourhood and becomes trapped in an otherwise empty bubble (Careri 1961). The radius of the bubble is determined by a balance between the zero-point energy of the confined electron and the energy associated with the surface of the bubble; it has a value of about 1.9 nm at low pressures.

At low temperatures the potential well described by equation (1.1) can be filled with ions up to a maximum areal density of $2\epsilon_0 E_0/e$ (typically about 10^{12} m^{-2}). The pools of ions so formed can be confined in the horizontal direction by a suitable fringing field, a suitable arrangement of electrodes being shown schematically in

figure 1. The frequency of small vertical oscillations of the ions in the potential (1.1) is typically about 50 MHz, so that at temperatures above about 2 mK the vertical motion of the ions is such that they are distributed thermally over a range of quantum states. The ion pools are not therefore strictly two dimensional. However, the spatial extent of the vertical motion is much smaller than the average spacing between ions, so that for many purposes the system is effectively two dimensional. The ions can be trapped for long periods only at sufficiently low temperatures; this is particularly true for the negative ion, which ceases to be trapped above about 1 K because the thermally excited vertical motion can then bring the ions sufficiently close to the surface for the electrons to tunnel out of the bubbles into the free space above the surface of the liquid (Schoepe & Rayfield 1973). As we shall prove later, the areal density in a trapped pool of ions is approximately uniform except where it falls rapidly to zero at a well-defined radius.

This paper is the first of a series that is concerned with a wide-ranging experimental and theoretical study of the behaviour of these pools of ions. Among the earliest experiments on such pools were those carried out by Poitrenaud & Williams (1972), who excited vertical oscillations of the ions in the potential well (1.1) at about 0.7 K and used the observed resonant frequencies to deduce effective ionic masses (about 243 m_4 for the negative ion and about 43.6 m_4 for the positive ion, where m_4 is the mass of the ^{4}He atom). Theobald *et al.* (1981) measured the horizontal response of a negative-ion pool to low-frequency oscillatory potentials applied to suitable electrodes surrounding the pool (see §§2 and 4), and they were able to reduce rough values for the mobility of the ions in the temperature range from 0.2–1 K. Ott-Rowland *et al.* (1982, 1983) excited two-dimensional plasma resonances in a positive-ion pool, and Barenghi *et al.* (1986), at an early stage in the present programme, reported the observation of similar resonances in pools of negative ions. Magnetoplasma resonances in pools of both positive and negative ions have been reported briefly by Mellor *et al.* (1988), again as part of the present programme.

The plasma resonances are of particular interest, and studies of them will form an important part of the present series of papers. The resonances involve motion of the ions in the horizontal plane, and they can be excited and detected with the electric circuit shown schematically in figure 1 and described in more detail in §2. In the absence of dissipation the dispersion relation for the plasma waves in a two-dimensional plasma of infinite extent is given by

$$\omega^2 = (n_0 e^2 k/2\epsilon_0 M) F(k), \tag{1.3}$$

$$F(k) = \frac{2 \sinh kd \sinh k(h-d)}{\sinh kh + (\epsilon - 1) \cosh kd \sinh k(h-d)}.$$

An outline proof is given for convenience in Appendix A; it relies on a combination of some simple electrostatics and an obvious linearized equation of motion for horizontal movement of the plasma ($\partial \boldsymbol{v}/\partial t = -(e/M)\nabla\phi$); n_0 is the areal density of ions (assumed constant in the absence of the plasma wave), M is the effective ionic mass, h is the vertical separation between the top and bottom electrodes shown in figure 1, and d is the height of the layer of ions above the bottom electrode. A circular pool of ions, such as is used in the present work, will exhibit plasma resonances at frequencies that depend on the boundary condition, which we discuss later, at the edge of the pool (this boundary condition will take account of the fact that the electrodes as well as the plasma are of finite extent). The resonances will be

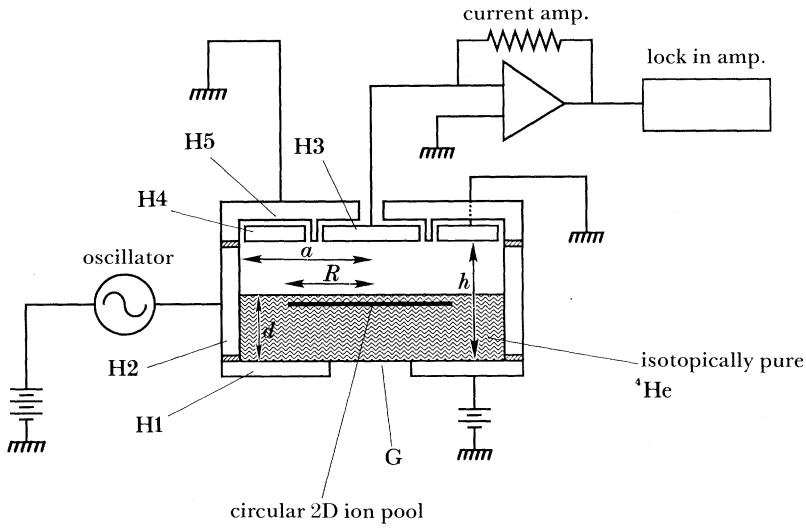

Figure 1. Schematic diagram of electrode assembly and circuit for the observation of plasma resonances. The electrode assembly has circular symmetry about a vertical axis.

reasonably sharp only if dissipation is sufficiently small; in practice, as we shall see, the dominant dissipative mechanism arises from interaction of the ions with the thermal excitations in the helium, an interaction that determines the mobility of the ions and which does indeed become sufficiently small at low temperatures.

We see that study of the plasma resonances will yield information about ionic masses and about the interaction of the ions with excitations of the helium; these excitations include not only the phonons and rotons that exist in the bulk of the liquid, but also the quantized waves, or ripplons, that exist at its surface. At high temperatures, where the plasma waves are highly damped, ionic mobilities can be obtained from the non-resonant response at the ion pool, as we shall describe later. These studies are, as we shall see, of considerable interest, but the ion pools are also of great interest for other reasons. For example, the ion plasmas are very cold, in the sense that the average potential energy of interaction between neighbouring ions is large compared with the average kinetic energy of an ion, so that two-dimensional (Wigner) crystals may form under the right conditions. The ions interact with the surface of the helium, and self trapping effects may arise, analogous to polaron formation in a three-dimensional electron–phonon system, although it should be emphasized that interaction with the surface is much weaker than is the case for electrons trapped above the helium surface. The plasma resonances can be studied in the presence of a magnetic field. Our earlier brief report of the observation of such magnetoplasma resonances (Mellor *et al.* 1988) will be followed by a more detailed account in a later paper in this series. The study of magnetoplasma resonances turns out to be of considerable interest, and, as we have already explained in our earlier report, it can yield much more reliable values of the ionic effective masses than can be obtained from equation (1.3).

This paper is arranged as follows. Our apparatus is described in some details in §2, and the computational procedures that we use to determine the densities and radii of our ion pools are described in §3. In §4 we present measurements of the low-frequency, non-resonant, response of our pools at high temperatures, and we show in

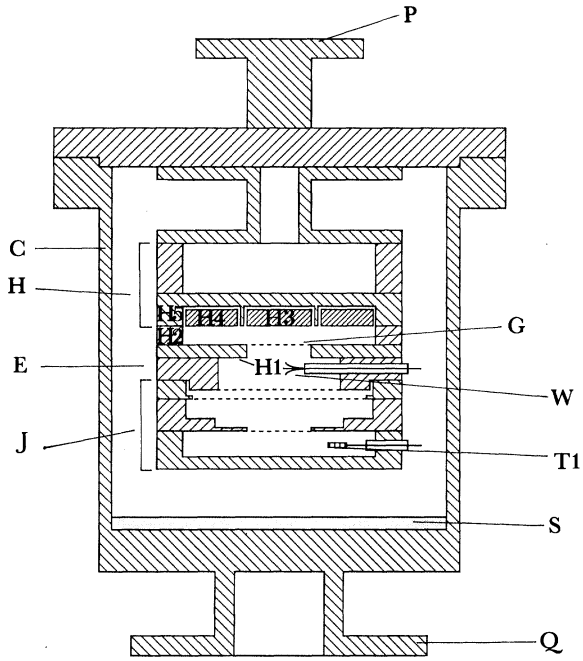

Figure 2. The experimental cell, containing the electrode assembly.

§5 how to deduce mobilities from these measurements. Sections 6 and 7 are devoted to the observation and analysis of the plasma resonances, and §§8 and 9 to measurements of plasma resonant damping and deductions from them of ionic mobilities at the lower temperatures. Section 10 deals with possible crystallization of our ion pools, and §11 summarizes our conclusions. A substantial part of the present paper is concerned with our measurements of ionic mobilities; the theory of ionic mobility will be discussed and developed in the next paper of this series, where a comparison of our measurements with this theory will also be presented.

2. The apparatus

A diagram of the experimental cell is shown in figure 2. It consists of a leaktight copper cylinder (C), containing the electrode assembly E. The top plate (P) of the cell is bolted to the mixing chamber of a dilution refrigerator, operating down to 9 mK, and a thermally shielded copper block (not shown), to which the main thermometers are attached, is bolted to the bottom flange Q. The electrodes are formed from gold-plated copper, except for the grids. In our early work the grids were formed from 38 μm phosphor-bronze mesh attached to the plates by silver paint, but the grid in the lower electrode H1 was later replaced by a specially made copper grid, similar to those used as specimen mounts in electron microscopes, soldered in position with Woods metal; with this latter type of grid the lower electrode has an upper surface that is more accurately flat than is possible with the mesh. Insulation between the plates is provided by 50 μm polyester film. The inner diameter of the ring electrode H2 is 30 mm, the spacing between the electrodes H3/4 and H1 is 3 mm, and the diameter of H3 is 10 mm. The cell is filled to the required level with ^{4}He through a narrow fill-line, the liquid level being monitored by measuring the capacitance

between appropriate pairs of electrodes. The ^{4}He used in the cell is isotopically pure, and other impurities are removed with suitable traps. Silver sinter (S) on the inside base of the cell ensures good thermal contact between the experimental helium, the mixing chamber and the thermometer block. The electrode assembly contains two sets of electrodes; an upper set (H), similar to that shown in figure 1 and labelled in the same way, and a lower set (J), designed for ionic time-of-flight experiments and not used in the present series of experiments. The application of a high voltage of appropriate polarity to the tungsten tips (W) creates the ions in the liquid, which are drawn towards the free surface of the helium through the grid (G) in the base electrode H1. Charging of the surface with positive ions proves to be possible at any temperature below about 1 K; in the case of negative ions charging seems to be possible only in the narrow temperature range between about 0.9 K and 1.1 K.

Two previously calibrated thermometers are attached to the thermometer block: a germanium resistance thermometer, calibrated over the range 9 K to 50 mK; and a set of superconducting samples (National Bureau of Standards (NBS) SRM-768) with calibrated transition temperatures of 208.04 mK, 162 mK, 99.95 mK, 23.05 mK and 15.57 mK, the transitions being located with a mutual inductance surrounding the samples. A third thermometer (T6) on the block is based on the susceptibility of a sample of CMN, measured from the observed frequency of a tunnel diode oscillator in the cryostat, the tank circuit of which contains a superconducting coil wound round the CMN; this thermometer is calibrated against the primary thermometers and is used particularly to interpolate between the lower fixed points of the NBS thermometer. Carbon resistance thermometers, based on small chips of Speer resistors, are used to monitor the temperature at various points in the system; one of these (T1) is placed in the helium in the experimental cell and another (T2), cut from the same resistor, is attached to the thermometer block. The thermometer T2 is calibrated against the primary thermometers or the CMN thermometer at the start of each run; the thermometer T1, assumed to have the same calibration as that of T2, serves to check that the experimental helium is at the same temperature as the thermometer block. We estimate that the measured temperatures of the helium in our experimental cell are accurate to within 1 mK.

The DC electrode potentials required to hold the ion pool in position are supplied from stabilized power supplies connected via four-stage *RC* low-pass filters with a time constant of about 1 s. In a typical experiment with positive ions the DC potentials on the electrodes are: the base electrode H1 at +15 V; the ring electrode H2 at +25 V; the upper circular inner electrode H3, the upper outer annular electrode H4 and the guard electrode H5 all at ground (0 V). For studies of the low-frequency non-resonant response of the ion-pool we use a Wayne–Kerr B221 capacitance–conductance bridge (operating at a frequency of 1.6 kHz), the voltage output from the bridge being applied to electrode H4 and the current input being taken from the electrode H3; electrode H5 remains grounded for both DC and AC to reduce the stray capacitance between H3 and H4. For studies of the plasma resonances an AC potential of variable frequency is applied to the ring electrode H2, and the charge induced on the electrode H3 is detected with a current preamplifier feeding a lock-in amplifier, as shown schematically in figure 1. The annular electrode H4 remains grounded. Because the plasma resonances can be very sharp, the oscillator must have good frequency stability, and most recently we have used a Hewlett-Packard 3325A synthesized frequency generator feeding the ring electrode through an attenuator and a 1 μF capacitor. The battery-operated current

preamplifier is made from a fast operational amplifier integrated circuit (ADLH0032CG) in a standard current amplifier configuration. Plasma resonance curves are plotted on an XY recorder, the output of the 9503-SC lock-in amplifier being fed to the Y input and a voltage proportional to the frequency of the generator being fed to the X input. After the measurements on a particular ion pool have been completed it is necessary to measure the total charge in the pool, for reasons that we explain later. To measure this total charge we connect electrodes H3 and H4 to the input of an electrometer, and measure the total charge induced on them when the potential on the base electrode H1 is reduced to zero. This induced charge has two components: one due to movement of the ions; and one due to the change in potential between the base electrode and the upper electrodes. The second component, which does not interest us, can be cancelled by restoring the potential on the base electrode to its original value.

As we have already explained, a finite ionic mobility leads to a damping of the plasma resonances. So that the observed damping can be used to determine the mobility, it is essential that there be no appreciable additional damping associated with the induced current flow in the circuits external to the cell. This means that the input resistance of these circuits viewed from the electrodes of the cell must be sufficiently small. In practice our circuits have been designed to satisfy this condition for mobilities less than 10^6 m^2 V^{-1} s^{-1}.

The behaviour of the ion pools proves to be very sensitive to vibration, and excessive vibration can even cause ions to be lost from the pool. The cryostat is therefore supported on anti-vibration mounts, and connections to pumps are made through suitable flexible tubing. Changes in electrical connections at the top of the cryostat are made remotely with reed switches, so that the cryostat need not be touched during measurements with a particular ion pool. As we shall see later, the behaviour of the ion pools is also extremely sensitive to the alignment of the free surface of the helium with the electrodes; the necessary adjustment is made using criteria to be described later by means of screws on the framework carrying the cryostat.

The electrical leads to the electrodes take the form of coaxial cables, both outside and inside the cryostat. The leads are such that they do not present impedances that are too high to either the external electronics or the experimental cell. This last requirement arises because, as we have already indicated, too large an impedance in the leads to the electrodes can give rise to unwanted damping of the ionic motion.

We have made measurements to verify that under operating conditions no significant temperature differences are set up between the thermometer block, the helium in the experimental cell, and the top of the experimental cell.

3. The static characteristics of the ion pool

To interpret our experimental measurements we need to know the equilibrium distribution of the trapped ions over the helium surface. This distribution is determined by the condition that the total horizontal component of the electric field acting on any ion shall vanish, this field being composed of that due to the potentials applied to the electrodes and that due to the charge distribution of the ions themselves. For the most part we have relied on numerical methods to solve this problem, as we describe below. Glattli *et al.* (1985) have published the results of an analytic solution, for the special case of a charge distribution midway between the

upper and lower electrodes ($d = \frac{1}{2}h$), the spacing (h) between the electrodes being much less than the inner radius of the ring electrode H2 (figure 1). Application of the Glattli *et al.* solution to our cell yields results that are within a few percent of those that we derive numerically, the small difference being due to use of a finite number of rings in our numerical work and the fact that the height of our cell is not sufficiently small compared with its radius.

One numerical method for solving our problem was described by Lambert & Richards (1981) in the context of the distribution of electrons above the surface of helium. We have chosen to use a rather different method, which includes a numerical simulation of the way in which any arbitrary initial charge distribution in the pool evolves in time; this simulation provides us with additional information, which will be useful to us later. We shall outline the method in this section, the details being given in Appendix B.

We assume that the dynamical behaviour of the pool is determined by the equation of motion

$$\partial v/\partial t + v\,\partial v/\partial r = (e/M\mu)\,v + eE/M \tag{3.1}$$

and the continuity equation

$$\partial\sigma/\partial t + (1/r)\,\partial/\partial r(r\sigma v) = 0, \tag{3.2}$$

where v is the radial drift velocity of the ions, σ is the charge density, and μ is the ionic mobility; we have assumed that the motion and distribution of ions in the pool is always axisymmetric. E is the radial component of the total electric field at the level of the ion pool; it is the sum of that due to the ion pool with grounded electrodes and that due to the potentials applied to the electrodes in the absence of the ions. To set up a numerical simulation we take the circular cross-section of the electrode assembly at the level of the ions and divide it into a large number, N, of concentric rings of equal width. The ionic charge density is taken to be constant within each ring, but may vary from ring to ring. In practice, N was taken to be 80; this number does not lead to the use of an excessive amount of computer time, and it is sufficient to produce an acceptable result (increasing the number from 80 to 110 changes the calculated charge density at the centre of a typical pool by only 0.04%). An initial charge distribution is specified by giving the charges on each ring, and initial velocities are taken to be zero. The electric field E is then computed. Numerical integration of the equation of motion, converted as far as spatial derivatives are concerned into a difference equation, leads to velocities, v, as functions of time, at all the ring boundaries, over a suitably small time-step. These velocities are then used, in conjunction with the continuity equation integrated over a ring and over the time-step, to compute the amount of charge that must be transferred across each ring boundary at the end of the time-step. The whole process is then repeated over another time-step with new initial charge and velocity distributions. This procedure will lead to the equilibrium distribution of ions after a time determined by the time constant $M\mu/e$. Corrections are made to allow for the fact that the dielectric constant of helium is not exactly equal to unity.

A typical equilibrium charge distribution obtained in this way is shown by the solid line in figure 3. We see that, as we anticipated in §1, the charge density is approximately uniform, except near the edge of the pool, where it falls rapidly to zero at a well-defined edge. Our results for equilibrium distributions are very similar to those obtained by Lambert & Richards, the detailed results for the same geometry differing by only a few percent. Small spurious spatial oscillations in the charge density found by Lambert & Richards are absent in our results.

PHILOSOPHICAL TRANSACTIONS OF THE ROYAL SOCIETY A MATHEMATICAL, PHYSICAL & ENGINEERING SCIENCES

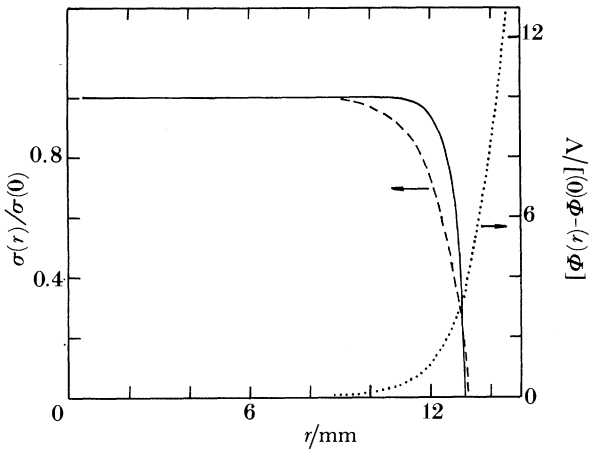

Figure 3. The charge distribution in a typical circular ion pool. Normalized charge density ($\sigma(r)/\sigma(0)$) plotted against radius (r). $n_0 = \sigma(0)/e = 3.14 \times 10^{11}$ m^{-2}. Electrode potentials: $V(\mathrm{H3}) = V(H4) = 0$; $V(\mathrm{H2}) = 25$ V; $V(\mathrm{H1}) = 15$ V. The full line is the result of using the full computational procedure described in outline in §3 and in detail in Appendix B. The dashed line is obtained from the simplified procedure that leads to equation (3.11). The dotted line is the potential $[\Phi(r) - \Phi(0)]$ at the level of the surface of the helium when no ions are present.

It is clear that, to find the charge distribution in any particular pool on which we have been performing experiments, we need to know the potentials on the electrodes and the total charge in the pool. As we explained in §2 we determine this total charge at the end of the experiments by measuring the charge induced on the upper electrodes of the cell by the ion pool. The relation between this induced charge and the total charge in the pool must again be found by numerical methods, which are also described in Appendix B. In practice, we are particularly interested in the radii of our pools and in the maximum ion densities in them. Therefore we use our numerical simulations to prepare graphs showing these two quantities as functions of the charge induced on the upper electrodes, for different sets of electrode potentials. These graphs are used in the subsequent analysis of our results.

The calculations that we have just described lead to a rather accurate description of the charge distribution within the static ion pool, but they fail to provide a clear physical understanding of the distribution. The following analysis may be helpful in this respect.

For simplicity of presentation we shall assume that the charge density, $\sigma(x)$, in the pool (situated in the plane $z = 0$) varies in only the x-direction. We shall also assume that upper and lower electrodes are situated in the planes $z = \pm\frac{1}{2}h$. The electrostatic potential $\phi(x)$ due to the charge distribution $\sigma(x)$ in the presence of the electrodes (held at zero potential) must be a linear function of $\sigma(x)$, and it can therefore be written

$$\phi(x) = \int \sigma(x')\, G(x - x')\, \mathrm{d}x'. \tag{3.3}$$

But we know from the analysis of Appendix A that the Fourier transforms $\phi(k)$ and $\sigma(k)$ are related by

$$\phi(k) = (2\pi)^{\frac{1}{2}} G(k)\, \sigma(k), \tag{3.4}$$

where

$$G(k) = (1/8\pi k^2 \epsilon_0^2)^{\frac{1}{2}} \tanh(\tfrac{1}{2}kh), \tag{3.5}$$

$G(k)$ being the Fourier transform of $G(x)$. It follows easily that

$$G(x) = (1/4\pi\epsilon_0) \ln[\{\cosh(\pi x/h) + 1\}/\{\cosh(\pi x/h) - 1\}], \tag{3.6}$$

where we have used the integral 4.114(1) in Gradshteyn & Ryzhik (1980). $G(x)$ has the limiting forms

$$G(x) \to (1/2\pi\epsilon_0) \ln (2h/\pi x) \quad \text{for} \quad x \to 0 \tag{3.7}$$

and

$$G(x) \to (1/2\pi\epsilon_0) \exp (-\pi x/h) \quad \text{for} \quad x \to \infty, \tag{3.8}$$

so that $G(x)$ has an effective range of order h.

Now suppose that $\sigma(x)$ does not vary significantly over a distance equal to the range h of $G(x)$. Then equation (3.3) reduces to

$$\phi(x) = \sigma(x) \int_0^\infty G(x')\, \mathrm{d}x' \tag{3.9}$$

$$= (h/4\epsilon_0)\, \sigma(x). \tag{3.10}$$

In practice, the electrodes are not held at zero potential. They are held at a potential that produces in the plane $z = 0$ a potential $\Phi(x)$. If the charge distribution $\sigma(x)$ is in equilibrium, then in the region where $\sigma(x) \neq 0$ we must have $\phi(x) + \Phi(x) = \text{const}$. It follows that

$$\sigma(x) = \sigma(0) - (4\epsilon_0/h)[\Phi(x) - \Phi(0)]. \tag{3.11}$$

We see that according to this approximate calculation the charge density in the ion pool can be obtained from the following model. Take a circular dish, the base of which has a height above some fixed level equal to $(4\epsilon_0/h)\, \Phi$, where Φ is the potential, obtained from numerical calculations, at the level of the surface of the helium due to the potentials on the electrodes when no ions are present. Pour a volume of water into the dish equal to the total charge in the pool. The resulting depth of water at any point in the dish is a measure of the charge density at the corresponding point on the liquid surface.

The results of applying this approximate method are shown by the dashed line in figure 3, where they can be compared with the results of our more accurate numerical computations. We see that, as we might have expected, the more exact calculation yields a profile that drops slightly more sharply at the edge of the pool, but that otherwise the two methods are in good qualitative agreement.

We emphasize that in the calculations described in this section we have assumed that the experimental cell and the liquid it contains have exact circular symmetry about a vertical axis through the centre of the cell. The ion pool must then be circular and coaxial with the electrodes. In practice, this assumption cannot be exactly correct. As we shall see later, some of our experimental results prove to be very sensitive to slight asymmetries, and it turns out to be very important to be aware of this fact. We shall find our dish-and-water model particularly useful when we come to analyse the effect of these asymmetries.

4. Measurements with the capacitance–conductance bridge

These measurements were made while the temperature of the experimental helium was drifting slowly, the bridge being balanced at selected temperatures. Checks were made that the results were independent of the direction of temperature drift, that the bridge voltage was sufficiently small to ensure a linear response of the ions, and, from the reproducibility of the results at a given temperature over a period of time, that no ions were being lost from the pool. A typical set of experimental results is shown in figure 4. We note that the results are sensitive to temperature only at the higher

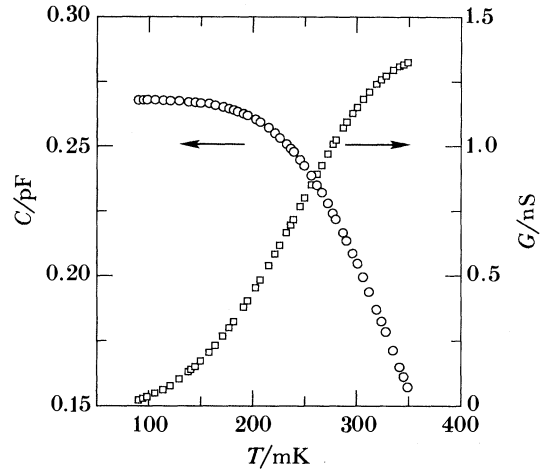

Figure 4. Capacitance, C, (○) and conductance, G, (□) of a pool of negative ions plotted against temperature, T.

temperatures, where the ionic mobilities are not too high; at the lower temperatures a high mobility allows the ions to respond quasistatically, giving rise to a temperature-independent capacitative response and negligible resistive loss.

5. Interpretation of the measurements with the capacitance–conductance bridge

The capacitance–conductance bridge measures the contribution of the ions to the impedance between electrodes H3 and H4, the impedance being expressed in terms of a capacitance and a conductance in parallel. The bridge works in such a way that H3 remains at earth potential, the bridge voltage being applied to H4. The frequency at which the bridge operates (1.6 kHz) is much less than any plasma resonant frequency of the pool.

To analyse the linear response of the pool to the voltage on H4, we note that any disturbance of the pool can be represented in terms of a linear superposition of its normal modes, and we assume that these normal modes are the plasma resonances of the pool. Since the system is assumed to be axisymmetric, we shall take into account only the axisymmetric resonances. As far as the bridge is concerned, each normal mode will act like a series resonant circuit across the bridge terminals, so that the pool can be represented by the circuit shown in figure 5, where R_i, C_i, and L_i refer to the ith plasma resonance and C_0 is the interelectrode capacitance in the absence of the ions. To determine the parameters defining each resonant circuit, we note first that

$$L_i C_i = 1/\omega_i^2, \tag{5.1}$$

where ω_i is the (undamped) angular resonant frequency of the ith plasma mode (determined, as we show in detail in §7, by the radius of the pool and the ionic density), and that

$$R_i/L_i = e/M\mu, \tag{5.2}$$

since this quantity is the time constant for free decay of the plasma mode. We still need one other parameter relating to each mode, and this is provided by a numerical computation of the C_is as follows. Suppose that we apply a steady perturbing potential to the electrode H4, electrode H3 remaining at earth potential. By using

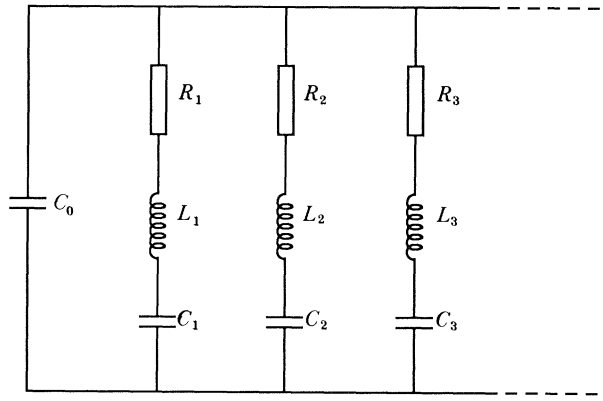

Figure 5. Equivalent electric circuit of the ion pool.

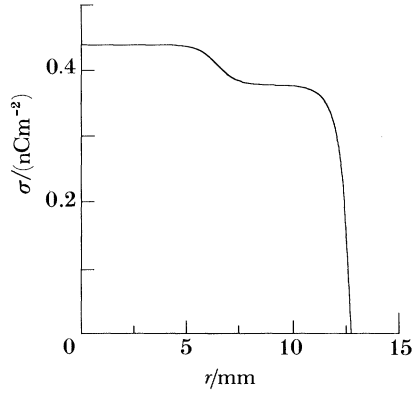

Figure 6. Perturbed equilibrium charge distribution in the ion pool after a perturbing potential is applied to electrode H4. Charge density, σ, plotted against radius, r. (V(H4) = 1 V; V(H3) = 0; V(H2) = 25 V; V(H1) = 15 V.

computational procedures similar to those used in the work described in §3 (see Appendix B), we calculate the perturbed ionic distribution; a typical result is shown in figure 6. This perturbation in the ionic distribution is analysed in terms of the normal modes, yielding an amplitude for each normal mode. Finally, a calculation is made of the charge induced on electrode H3 by the perturbation in the ionic density corresponding to the ith mode, and the ratio of this charge to the steady perturbing potential applied to H4 is the required value of C_i.

For a pool of known radius and charge density this procedure will yield the impedance presented to the capacitance–conductance bridge in terms of the mobility μ. Measurements of this impedance, such as those illustrated in figure 4, can then be used to deduce the ionic mobility as a function of temperature. As we have already noted, however, the impedance is sensitive only to low mobilities, and therefore, as we shall see more clearly later, the method works only at rather high temperatures. The mobilities that we have obtained by this method are presented in §9.

6. Observation of plasma resonances

As we explained in §1 the ion pools can support plasma resonances, in which the motion of the ions is horizontal. For the resonances to be sufficiently sharp to be

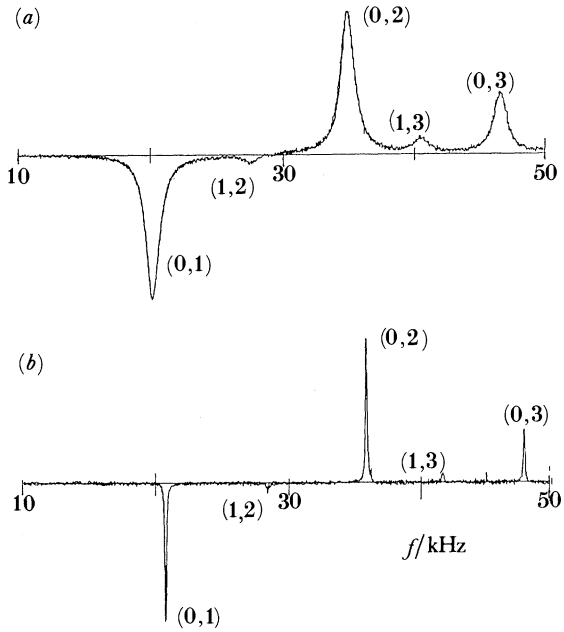

Figure 7. Plasma resonances in a pool of negative ions. Response of the pool plotted against frequency for two temperatures. (*a*) $T = 81$ mK, (*b*) $T = 54$ mK.

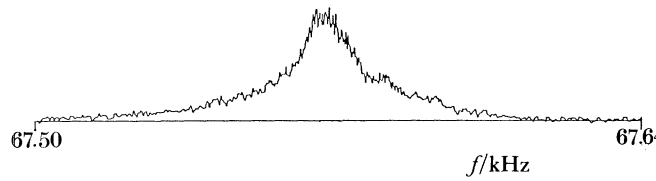

Figure 8. The (0, 1) plasma resonance in a pool of positive ions at a temperature of 10 mK. Response of the pool plotted against frequency.

resolved the ionic mobility must be sufficiently large, and this condition is satisfied if the temperature is less than about 300 mK for positive ions and about 100 mK for negative ions. The resonances can be generated and detected by the means described in §2. It turns out that the resonant response is linear only if the ionic velocity amplitude is less than about 0.1 m s^{-1} for positive ions or 1 m s^{-1} for negatives. In this paper we shall confine ourselves to the linear response. The nonlinear effects have already been described briefly by Ott-Rowland *et al.* (1982, 1983) for positive ions and by Barenghi *et al.* (1986) for negative ions, and they will be discussed in detail in a later paper in this series.

Typical experimental resonance curves at fairly high temperatures are shown in figure 7. The different allowed modes are specified by a pair of numbers (m, n), as explained in the next section. The rapidly increasing Q with decreasing temperature reflects a rapidly increasing ionic mobility, as will be discussed in more detail later. The (0, 1) resonance at the very low temperature of 15 mK is shown in figure 8. Resonant frequencies and resonant linewidths have been obtained by drawing smooth lines through the observed resonance curves, and it has been checked that these curves have a lorentzian shape.

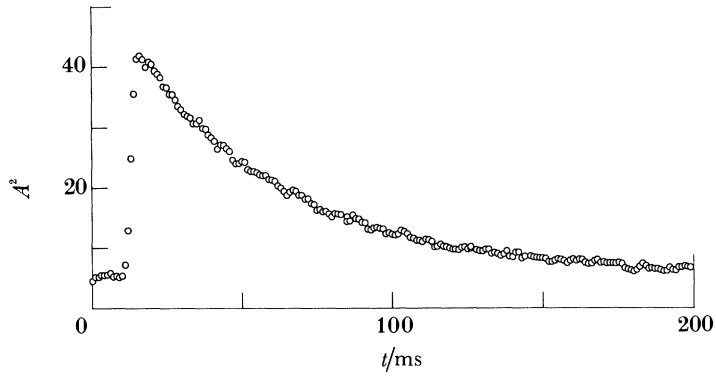

Figure 9. Free decay of plasma oscillations in a pool of positive ions. The square of the amplitude of oscillation, A (in arbitrary units), of the $(0, 1)$ mode plotted against time, t, for a temperature of 15.5 mK and trapping depth 72.5 nm.

We have experienced difficulty in measuring linewidths at the lowest temperatures. The resonances are clearly subject to some form of disturbance, which has a serious effect when, at low temperatures, the resonances are very narrow (figure 8). Such a disturbance was first noted by Ott-Rowland *et al.* (1982), who found that it took the form of a periodic shift in the resonant frequency due to a wave motion on the surface of the helium. Such a wave motion is presumably excited by residual vibration of the cryostat, and it affects the plasma resonant frequency for reasons similar to those discussed below in connection with the effect of tilting the cryostat. In our own case the disturbance is sometimes of this same type, but at other times it seems to be different in character, giving rise to irregular shifts in the resonant frequency and sometimes to what appears to be a genuine, but irregular, broadening of the resonance.

To measure the damping of very sharp resonances in the presence of irregular shifts of the resonant frequency, we have developed a technique in which we measure the time constant associated with the free decay of the plasma resonances. The pool is driven periodically by short (typically 2 ms) RF pulses at its resonant frequency, and the signal from electrode H3 due to the freely decaying oscillations between pulses is amplified and fed to a lock-in detector. The reference signal for this detector is the CW RF signal from which the RF pulses are derived, and its time constant is chosen to be sufficiently short that its output reflects with reasonable accuracy the envelope of the freely decaying plasma oscillations. In practice the 'in phase' and 'quadrature' outputs of the lock-in detector are read by a computer at sufficiently frequent intervals, the two resulting digital signals are squared and added, care being taken to eliminate any offsets on the two outputs, and the resulting signal is then subjected to digital averaging over enough pulses to yield an acceptable signal to noise ratio. This resulting signal is the envelope of the freely decaying plasma oscillation (modified a little by the finite bandwidth of the lock-in detector), even if the frequency of the reference signal has drifted away from that of the plasma, although it must not have drifted by more than the bandwidth of the lock-in detector. A typical free decay obtained in this way is shown in figure 9. The time constant associated with the decay in the amplitude of the plasma oscillation is related to the full-width at half height of the resonance curve by the relation $\tau = 2/\Delta\omega$. (Strictly speaking, the fitting procedure used to extract τ uses two

exponentials: one based on τ, and the other on the bandwidth of the lock-in detector.)

As we mentioned in §2 we take care to level the cryostat before taking measurements on the ion pools, the levelling being necessary to ensure that the liquid surface, and therefore the plane of the ion pool, are parallel to the upper and lower electrodes of the cell. As we have already reported briefly (Mellor *et al.* 1988), the measured plasma resonant frequencies prove to be very sensitive to this alignment, for reasons that we shall discuss in the next section. It seems very likely that this sensitivity means that the resonant frequencies are also very sensitive to any small misalignment of the electrodes. Although the cell was constructed with care, such a small misalignment may have been present in the cell during the measurements reported here, with resulting small errors that we mention in the next section.

7. The plasma resonant frequencies and the ionic effective masses

To predict the plasma resonant frequencies we need to know the effective boundary condition obeyed by a plasma wave at the edge of the pool. This effective boundary condition must take account of three factors: the finite extent of the pool; the fact that the equilibrium plasma density is not spatially constant near the edge of the pool; and the finite lateral extent of the electrodes, including the presence of the ring electrode H2. One way of obtaining the approximate boundary condition is from a study of the results of the numerical simulations described in §3. The simulated dynamical evolution of the pool is computed for a variety of initial perturbations, and attention is focused on the behaviour of the edge of the pool. We find that the edge moves very quickly to its equilibrium position, the rest of the perturbation then decaying relatively slowly while the edge remains fixed. This suggests that the boundary condition relevant to the relatively low-frequency oscillations with which we are concerned is that the edge of the pool is fixed, at least to a good approximation. A physical picture of this boundary condition can be obtained from the simplified analysis given in §3: the potential $\Phi(x)$ rises very sharply at the edge of the pool and this leads to an effective clamping of this edge. For the purposes of the present discussion we shall first assume that the boundary condition is that the edge of the pool is fixed, but we shall make appropriate corrections later.

As shown in Appendix A, the perturbed charge density associated with a plasma resonance in a circular pool of uniform density held between electrodes of infinite lateral extent has the form

$$J_m(kr)\exp(\mathrm{i}m\theta), \tag{7.1}$$

where $J_m(x)$ is a Bessel function of order m. We specify a particular mode of oscillation by the numbers (m, n), where $k_1, k_2, k_3, \ldots, k_n, \ldots$ are the successively increasing values of k that are allowed by the boundary condition at the edge of the pool: in the approximation that we take the density of the pool to fall abruptly at its edge, that the edge of the pool is taken as fixed, and that we ignore the finite lateral extent of the electrodes, the k_ns are given by the condition that the velocity at the pool edge ($r = R$), derived from (7.1), shall vanish, i.e.

$$[(\mathrm{d}/\mathrm{d}r)\{J_m(kr)\}]_{r=R} = 0. \tag{7.2}$$

(This is equivalent to the condition (A 22) in Appendix A, when $\omega_c = 0$.) The frequencies of the modes are given in terms of the k_is by equation (1.3). The

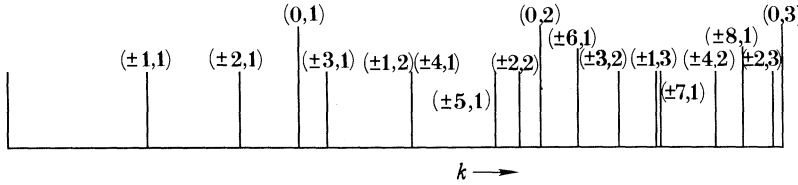

Figure 10. Diagram showing the wavenumbers of the first 31 resonant modes of a circular ion pool. The wavenumber of the (0, 3) mode is typically about 10^3 m^{-1}.

Table 1. *Comparison between the measured resonant frequencies for negative ions and those predicted by the dispersion relation*

(Normalized to the frequency of the (0, 1) mode.)

mode (m, n)	measured frequency kHz	predicted frequency kHz
(0, 1)	22.10	22.10
(1, 2)	30.37	29.90
(0, 2)	38.37	37.88
(1, 3)	44.62	44.36
(0, 3)	51.36	50.61
(1, 4)	56.72	55.86
(0, 4)	61.63	60.87
(1, 5)	66.17	65.21
(0, 5)	70.49	69.37
(0, 6)	77.83	76.66
(1, 7)	81.16	79.92

frequencies of the first 31 modes for our system are shown schematically in figure 10. Modes with $m \neq 0$, which are doubly degenerate, lack axial symmetry, and therefore our system should neither excite them nor detect them; the fact that weak responses corresponding to some of these modes are evident in figure 7 must be due to some departure of the geometry of our cell from perfect axial symmetry at the time that these observations were made.

As we have emphasized, this analysis can be only approximately correct. A more accurate analysis, which takes account of the factors that we have ignored, has been given by Prasad & Morales (1988; referred to later as PM). Their figure 6 shows the extent to which our analysis is inaccurate; it shows that our analysis yields resonant frequencies that are too large by between 2 and 5% in the range of values of kR to which our observations relate.

Confirmation that the dispersion relation (1.3), together with the appropriate boundary condition, does indeed describe our experimental results is shown in table 1, in which the observed resonant frequencies for negative ions *relative* to the (0, 1) mode are compared with theory, taking into account the PM corrections. (We have not carried out a similar check for the positive ions because the frequencies of the higher modes are then greater than can be handled by our electronics.) We have also confirmed experimentally the dependence of the resonant frequencies on n_0 indicated by (1.3). The *absolute* frequencies depend of course on the effective mass of the ions concerned, and we turn now to the values of these masses that can be obtained from the observed resonant frequencies.

It can be stated immediately these masses are in at least rough agreement with those deduced from other experiments. However, it turns out, as we shall now explain, that masses obtained from our observed plasma resonant frequencies, which we shall refer to as 'plasma masses (M_p)', are subject to an unexpected uncertainty (Mellor *et al.* 1988).

That this uncertainty exists came to our attention when we discovered that the observed plasma resonant frequency decreases with increasing magnitude of the holding field E_0, to an extent that depends strongly on the levelling of the experimental cell; typically the resonant frequency decreases by about 1.9% when E_0 is increased from 5 to 21.7 kV m^{-1} at an angle of tilt of about 3 mrad. (The field E_0 is changed by changing the potential applied to the base electrode H1, but the potential applied to the ring electrode H2 is changed at the same time in such a way that the pool radius – and therefore the ion density – remains constant.) We believe that this effect arises as follows. When the cell is tilted, the surface of the helium, and with it the plane containing the ions, becomes inclined to the top and bottom electrodes of the cell, so that the field E_0 acquires a component parallel to the plane of the ions. As we show in Appendix C, the existence of this component has little effect on the position or shape of the ion pool, but it does introduce a gradient in the ion density across the pool, and this leads in turn to a shift (actually a reduction) in the plasma resonant frequency that increases with increasing E_0; for a given angle of tilt the predicted reduction in frequency as E_0 is increased is in at least rough agreement with experiment. (We did not make a direct experimental check on the dependence of the resonant frequency on tilt at fixed E_0; this was because a change in the tilt of the cryostat invariably led to a loss of ions from the pool, so that such a direct check would have required a measurement of the charge in the pool, and hence a recharging of the pool, for each angle of tilt. The charge in the pool cannot be determined with sufficient precision for such a measurement to be significant.) We note that the observed decrease in plasma resonant frequency with increasing holding field might be interpreted as an increase in effective mass of the ions with a decrease in the depth at which they are held below the surface of the helium. Such an interpretation was suggested by S. Hannahs & G. A. Williams (unpublished work), although later they agreed that the effect does not reflect a real change in effective mass (G. A. Williams, personal communication). In their apparatus they found that the effect is associated with an overlap of the edge of the ion pool with the meniscus rise in the helium level at the wall of the containing cell, which leads again to a distortion in the profile of the ion density. Evidence that the effective mass of the ions does not vary with depth, under the conditions of the present experiments, has been provided by measurements of the ionic cyclotron mass; a short report of this work was given by Mellor *et al.* (1988), and a full report will be included in a later paper in the present series.

The theory of Appendix C suggests that the plasma resonant frequency should not depend on the holding field if the cell is horizontal, provided of course that there is no genuine change of effective mass with depth. In practice, in our experiment, the dependence on holding field is minimized when the cell is horizontal, but it is not completely absent. This is probably due to the fact that the upper and lower electrodes in our cell are not exactly flat, so that in no orientation of the cell is the field E_0 normal to all areas of the ion pool. During the course of our work we did in fact reconstruct the cell in a way that ought to have made it geometrically more perfect, and this did result in a reduction in the dependence of the plasma resonant

PHILOSOPHICAL TRANSACTIONS OF THE ROYAL SOCIETY A MATHEMATICAL, PHYSICAL & ENGINEERING SCIENCES

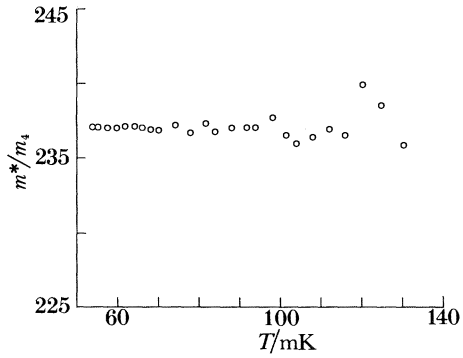

Figure 11. The temperature dependence of the effective mass of the negative ion, determined from the temperature dependence of the plasma resonant frequency. Ionic effective mass, in units of the mass of the ^{4}He atom, plotted against temperature, T.

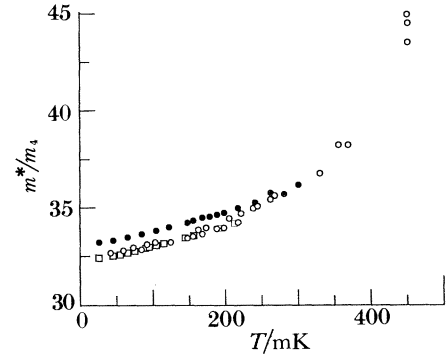

Figure 12. The temperature dependence of the effective mass of the positive ion, determined from the temperature dependence of the plasma resonant frequency. Ionic effective mass, in units of the mass of the ^{4}He atom, plotted against temperature, T. The different symbols refer to results obtained with different pools; the differences reflect errors in the measurement of the total charge in each pool and hence of the pool charge density and pool radius.

frequency on holding field. However, some imperfection remains. As a consequence the effective masses that we deduce from the plasma resonant frequencies will be subject to an unknown systematic error, although this error will be minimized at the lowest values of the holding field. The fact that non-axisymmetric modes are always seen, albeit in our latest cell with very small amplitude, is also an indication that some geometric imperfection is still present.

Values of the effective masses for the positive and negative ions derived from the plasma resonant frequencies at a holding field of 5 kV m^{-1} and at a temperature of 50 mK are about 33 m_4 and about 237 m_4. Both values are subject to an experimental error of about $\pm 5\%$, which has its origin largely in our measurement of the total charge in the pool, from which we derive its radius and charge density as described in §3. The temperature dependence of the plasma effective mass, but not its absolute value, can be determined more accurately by observing how the plasma resonant frequency of a particular mode in one particular pool varies with temperature, and this is shown for the two species of ion in figures 11 and 12. Within the experimental error the mass of the negative ion does not depend on temperature, although the error becomes fairly large at the higher temperatures where linewidths are large.

However, the plasma mass of the positive ion does exhibit a strong temperature dependence, an effect that was first reported by Ott-Rowland *et al.* (1982) and confirmed in both the plasma mass and the cyclotron mass in our own early experiments (Mellor *et al.* 1988). The most recent absolute values of the plasma effective mass of the positive ion obtained by the UCLA group (Hannahs & Williams 1987) are slightly smaller than our own, but hardly outside the combined experimental errors. We remark that the cyclotron mass can be determined much more accurately than the plasma mass (Mellor *et al.* 1988), although it is possible that the two masses should not be exactly equal. We shall compare our measured masses with theoretical expectations in the later paper in this series that deals with our studies of magnetoplasma effects.

Our values for the plasma effective masses can be compared with those obtained by Poitrenaud & Williams (1972) from a measurement of the resonant frequency at which an ion can vibrate in a vertical direction at the bottom of the potential well described by equation (1.1). These 'vertical masses', M_v, were measured at a temperature of about 700 mK: for the negative ion a value of $(243 \pm 5)\, m_4$ was reported (where m_4 is the mass of the helium atom); for the positive ion the value was $(43.6 \pm 2)\, m_4$. For the negative ion there is good agreement with our plasma mass, although both are about 5% more than the cyclotron mass reported by Mellor *et al.* (1988). An apparent plasma mass that is too high could well be due to the 'tilt effect' described earlier in this section, and we believe the cyclotron mass to be the more reliable. The agreement between the M_v at 700 mK and the plasma mass at low temperatures may therefore be due either to an error in M_v or to a small increase in the effective mass of the negative ion with increasing temperature. Our values of the plasma mass of the positive ion are again larger, now by about 7%, than the corresponding cyclotron mass, and again we believe the cyclotron mass to be the more reliable. The strong temperature dependence of the mass of the positive ion and the fact that our measurements do not extend above about 300 mK render difficult any useful comparison of our values with that obtained for M_v.

It is of considerable interest to discuss the possible origin of the strong temperature dependence of the effective mass of the positive ion at the low temperatures with which the present studies are concerned. (A temperature dependence observed at much higher temperatures by Dahm & Sanders (1970) was probably associated with drag of the normal fluid.) We note first that the effective masses of the two ions are not affected by proximity to the surface of the helium (the best evidence comes from the measured cyclotron masses), so that it is reasonable to assume that the effect would be present in bulk helium and is not due to, for example, ripplon interactions. At first sight the effect appears to be peculiar to the positive ion. This must indeed be the case if the mechanism underlying the effect were to give rise to a change in mass that is proportional to the mass itself, since such a situation would obviously lead to a change in mass of the negative ion that is much larger than is observed. However, if the mechanism were to give rise to an enhancement of the mass by an amount that is independent of the mass of the ion, the change in mass of the negative ion between, say, 30 mK and 130 mK would be expected to be about $1 \times m_4$, which amounts to only about 0.5% of the total negative ion mass. Such a small change is within our experimental error.

Three recently published theoretical papers are relevant to our problem. The first, by Putterman *et al.* (1988), discusses the expected velocity dependence of the effective mass of an ion moving in superfluid helium. If the helium were an

incompressible classical fluid, then the effective mass is independent of velocity and equal to the mass of the 'bare' ion (i.e. the mass of the bare sphere of solid helium in the case of the positive ion, or the mass of the bare bubble in the case of the negative ion) enhanced by half the mass of the fluid displaced by the ion (see, for example, Landau & Lifshitz (1959, p. 36), where the 'bare' ion is regarded as a rigid sphere moving through the fluid). However, for a compressible fluid the mass enhancement is velocity dependent to an extent that depends on the square of the ratio of the speed of the ion to the speed of sound in the fluid. Such an effect could give rise to nonlinear responses in the plasma resonances, which we shall discuss in a later paper, but it can also give rise to a temperature dependence of the effective mass measured in the linear plasma response, if account is taken of the thermal velocity of the ions. Putterman *et al.* show that this effect will be described by the equation

$$M(\mathrm{T}) = M(0) + (21/20)\,[2\alpha/(2+\alpha)]\,k_{\mathrm{B}}\,\mathrm{T}/c^2), \tag{7.3}$$

where α is the ratio of the mass of displaced fluid to the bare ionic mass, and c is the speed of sound in the helium. The resulting change in mass with temperature is much less than that observed for the positive ion, so that we must conclude that the effect discussed by Putterman *et al.* is not responsible for most of the observed temperature dependence of the positive ion. The mechanism would of course operate on both types of ion, although in the case of the negative ion the predicted change with temperature is too small to have been observed in our experiments.

We note that the temperature-dependent mass enhancement described by Putterman *et al.* could be described in terms of the formation of virtual phonons around the ion. In reality, virtual rotons could also form. Since the roton wave velocity, c_{R} (*ca.* 60 m s^{-1}), is much less than the speed of sound (*ca.* 238 m s^{-1}), the effect of such rotons is likely to be much larger, perhaps by a factor of about c^2/c_{R}^2, which is equal to 15.7. This factor is not large enough (by a factor of about 30) to give agreement with experiment, but a detailed calculation of the effect of virtual roton creation is required to assess the importance of this mechanism properly. As we understand it, such a calculation is the one published recently by Tao Pang (1988, 1990); it suggests that the mechanism could indeed account for the experimental results, although the paper has been criticized by Elser & Platzman (1990).

The third theoretical paper is that of Elser & Platzman (1988), who propose a mechanism that operates only on the positive ion. They point out that the solid core of the positive ion contains only a small number of atoms (roughly 20), so that it might consist of 'nucleus' formed from a He_2^+ ion surrounded by a single shell of He atoms. Such an object may not be spherical; it might, for example, have roughly the form of an ellipsoid of revolution, the axis of which is determined by the orientation of the He_2^+ nucleus. Such an object has an anisotropic effective mass, since the contribution to this mass from the surrounding fluid backflow depends on the direction of motion of the ellipsoid relative to its axis of revolution. At the temperatures with which we are concerned, both translational and rotational motion will be thermally excited. In the case of an ellipsoidal ion these two types of motion will interact and give rise to an average effective mass for linear motion that depends on the degree of excitation and therefore on the temperature. Elser & Platzman show that a ratio of the major to the minor axes of the ellipsoid equal to about 1.21 would lead to a temperature dependence in the effective mass that is consistent with that observed.

It is clear that the temperature dependent effective mass of the positive ion is

likely to be related to the nonlinear response of the plasma, since a change of effective mass with ionic velocity would lead to a shift in resonant frequency with amplitude. We shall be discussing this nonlinear response in detail in a later paper in this series, where we shall continue our discussion of the temperature dependence of the ionic effective mass.

We must now refer to the occasional observation of an apparent splitting of some of the plasma resonances. The effect has been seen only with positive ions, and it was first observed with the (0, 1) resonance, which should be non-degenerate. Over certain ranges of electrode potentials (either the base electrode, H1, or the ring electrode, H2) the resonance can apparently split into two. At one extreme value of the appropriate electrode potential one of the two modes has a very small amplitude; as the electrode potential is changed to its other extreme value the two modes first move together in frequency and then move apart, while at the same time the relative amplitudes of the modes are interchanged. This behaviour is strongly suggestive of mode crossing. It is unaffected by temperature, and it has been seen also in the (1, 2) resonance but not in the (0, 2) resonance. The effect is not reproducible from one experimental run to another or even from day to day during a single run. We cannot be sure of the origin of the effect, but we suspect that it arises as follows. We see from figure 10 that different modes of the ideally circular pool of uniform density are often quite close in frequency; the (1, 2) and (4, 1) modes are very close, while the (0, 1) and (3, 1) are fairly close. If, because of some imperfections in our cell, the pools that we produce are not exactly circular or do not have exactly uniform density the mode frequencies may be shifted, and they might be caused to cross as the potential on a particular electrode is changed. One imperfection, to which we have already had occasion to refer, arises if the experimental cell is not exactly horizontal; the extent to which the cell departs from an exactly horizontal setting is likely to vary from run to run, so that the lack of reproducibility of the effect is not surprising. The existence of the effect adds weight to our contention earlier in this section that reliable values of the absolute effective ionic masses cannot be obtained from the observed plasma resonant frequencies.

It was suggested by Williams & Theobald (1980) that below a certain temperature the effective mass of an ion trapped below the surface of superfluid helium might be enhanced by distortion of the liquid surface above the ion; i.e. by formation through ion–ripplon interactions of the analogue of the polaron that can be produced by electron–phonon interactions in a three-dimensional crystal. Our results show no such effect with either positive or negative ions in the temperature range that we have so far studied. It should be emphasized that the calculation of Williams & Theobald relates to an isolated ion; in our experiments the effect would be modified by the formation of a Wigner crystal, which we discuss in §10.

8. Plasma resonant linewidths

These linewidths are determined by the damping of the plasma waves, and such damping can arise in two ways: from drag on the motion of an individual ion as it moves through the superfluid helium; and from viscous damping in the plasma itself. The first effect can be described in terms of an ionic mobility, μ, which gives rise to a lorentzian broadening of the in-phase response with a linewidth (full width at half height) given by

$$\Delta\omega = e/M\mu. \tag{8.1}$$

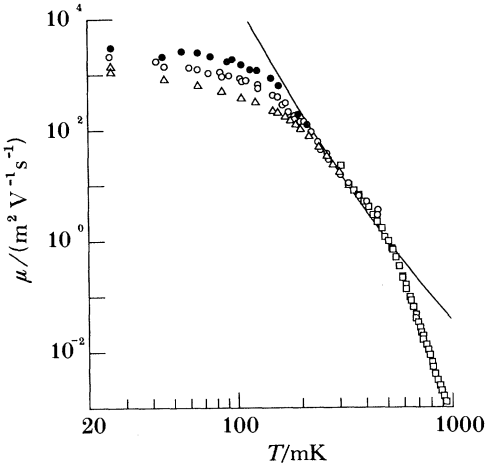

Figure 13. Temperature dependence of the mobility, μ, of the positive ion. The solid line is the theoretical prediction for the phonon-limited mobility, to be discussed in a later paper. Measurements with the capacitance conductance bridge: □, $z_0 = 43.5$ nm. Measurements of plasma wave damping: ○, $z_0 = 43.5$ nm; ●, $z_0 = 56.1$ nm; △, 36.7 nm.

We expect the mobility to be independent of frequency, so that the linewidth ought also to be independent of frequency. (We have defined the mobility in terms of the drag on a moving ion, not in terms of the velocity of the ion induced by an applied electric field; at a finite frequency, ω, this latter response, but not the drag force, is modified by a factor $1/(1-i\omega\tau)$, where τ is the momentum relaxation time for the ion.) If dissipation within the plasma itself can be described in terms of a (two-dimensional) viscosity, η, then such dissipation will give rise to an additional contribution to the linewidth, given by

$$\Delta\omega_v = \eta k^2/Mn_0, \tag{8.2}$$

which exhibits a strong frequency dependence. We have made measurements on the different resonant modes of our pools, and these have enabled us to show that, within our experimental error, our linewidths exhibit no frequency dependence. It follows that under the conditions of our experiments the dominant damping mechanism in the plasma waves is that associated with the finite ionic mobility (the theoretical significance of this result will be discussed in a later paper). We can therefore use our experimentally determined linewidths, in combination with equation (8.1), to obtain ionic mobilities, and we can thus extend the measurements described in §5 to much lower temperatures.

9. The ionic mobility

The results of the procedures described in §§5 and 8 are shown in figures 13–17. In figures 13 and 14, which relate to temperatures above about 30 mK, we have plotted the measured mobility for the positive and negative ions respectively against the temperature for various values of the depth, z_0, at which the ions are held below the surface of the helium. We see that the data obtained by the two methods (non-resonant response of the pool at high temperatures; plasma resonant linewidths at low temperatures) are in good agreement in the region of overlap. At the higher temperatures (greater than 270 mK for negative ions; greater than 370 mK for

PHILOSOPHICAL TRANSACTIONS OF THE ROYAL SOCIETY A MATHEMATICAL, PHYSICAL & ENGINEERING SCIENCES

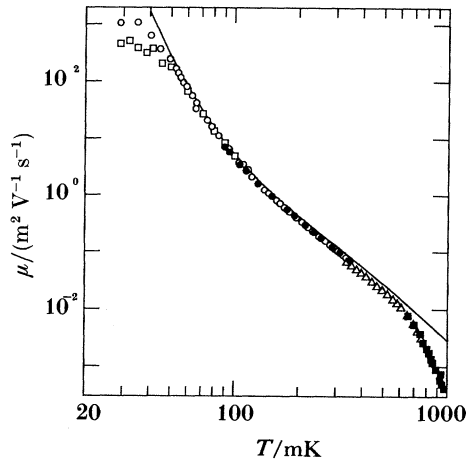

Figure 14. Temperature dependence of the mobility, μ, of the negative ion. The solid line is the theoretical prediction for the phonon-limited mobility, to be discussed in a later paper. Measurements with the capacitance conductance bridge: ■, △, ⬣; $z_0 = 43.5$ nm (different runs). Measurements of plasma wave damping: ○, $z_0 = 43.5$ nm; □, $z_0 = 20.5$ nm.

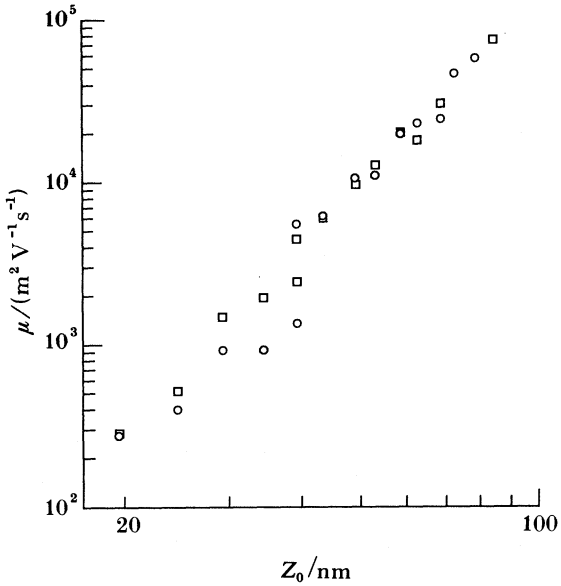

Figure 15. Dependence of the mobility, μ, of the positive ion on the depth, z_0, at which the ions are trapped below the liquid surface, at a temperature of 15 mK. □, from the (0, 1) mode; ○, from the (0, 2) mode.

positives) our results can be compared with those obtained by time-of-flight techniques by Schwarz (1972*a*), and we find that there is good agreement. We note that the mobility becomes dependent on z_0 at the lowest temperatures, this effect being shown in greater detail for positive ions in figure 15, where we have plotted the mobility against z_0 for a temperature of 15 mK. In the temperature range where the mobility is strongly dependent on z_0 the inverse mobility is closely proportional to the temperature, as is shown for positive ions in figure 16. The measurements in

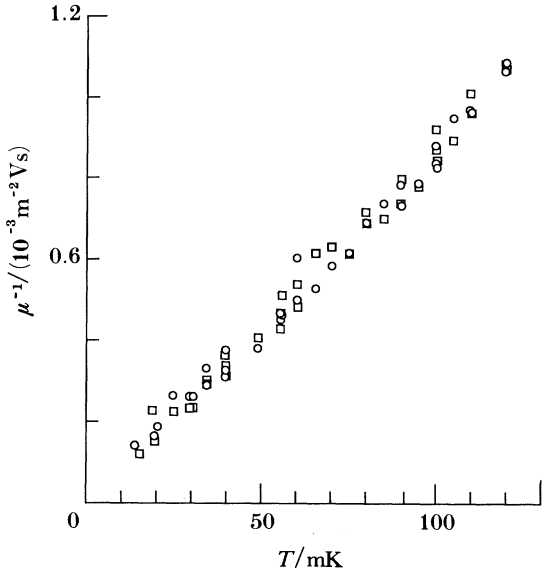

Figure 16. Temperature dependence of the inverse mobility, $1/\mu$, of the positive ion at very low temperatures ($z_0 = 43.5$ nm). ○, from the (0, 1) mode; □, from the (0, 2) mode.

figure 15 yield a dependence of mobility on depth as z_0^w, where $w = 3.5 \pm 0.2$, if account is taken of only the (probably more accurate) data based on the free decay of plasma oscillations; if all the data are included w falls to 2.8 ± 0.5. Most of the data for very low temperatures displayed in figures 15 and 16 were obtained from the free decay of plasma oscillations, as described in §6.

The results in figures 13–16 refer to pools of fairly high density (greater than 2×10^{11} m^{-2}), for which the mobility is found to be at least approximately independent of density. At low temperatures, in pools of low density, we find some evidence that the measured mobilities decrease with decreasing density, as shown in figure 17. However, under these conditions the signals from the pools are small and are badly affected by the vibrations mentioned in §6, so that this apparent dependence of mobility on density may not prove to be real. A similar effect has been reported by Hannahs & Williams (1987), but the fact that their results are not in quantitative agreement with our own (the effect seen by them is much larger) lends some support to the view that the effect may not be real. We are carrying out further experiments to clarify the situation.

We shall discuss in detail the theoretical interpretation of our observed ionic mobilities in later papers in this series, but it may be helpful to summarize our conclusions at this point. The mobilities are limited by scattering from three types of excitation in the helium: rotons, phonons and ripplons (our helium is isotopically pure, so that scattering from ^{3}He atoms can be neglected). At the highest temperatures covered by the present measurements (near 1 K) scattering by rotons is dominant, and this process has been the subject of detailed experimental and theoretical study many years ago (see, for example, the review by Schwarz (1975)); our results add nothing new. At somewhat lower temperatures scattering by phonons becomes dominant; the theory of this process was developed by Baym *et al.* (1969) and by Schwarz (1972*b*), but the present work provides what is probably the first set of experimental data that can be used to subject this theory to a rigorous test. The

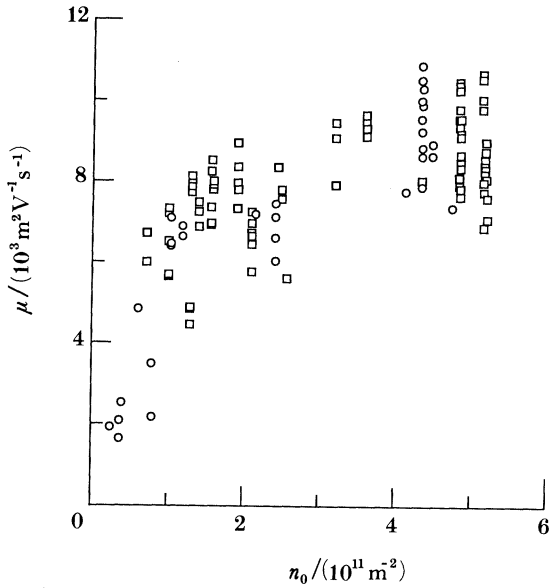

Figure 17. Dependence of the mobility, μ, of positive ions on density, n_0, of the pool at a temperature of 15 mK and $z_0 = 43.5$ nm. The circles and squares refer to different series of runs.

theory of the phonon-limited mobility will be discussed and developed in detail in the next paper in this series, where we shall show that it leads to very good agreement with experiment for the negative ions and fairly good agreement for the positive ions.

At the lowest temperatures the mobility depends, as we have shown, on the depth at which the ions are trapped below the surface of the helium, which suggests strongly that the mobility is becoming limited by the ripplons. (The phonon-limited mobility can in principle depend on the trapping depth, owing to the interference between a phonon and its reflection from the free surface (Shikin 1970), but, as we shall demonstrate in the next paper in this series, the resulting depth dependence is much smaller than is observed.) We are presently developing a theory of ripplon-limited mobility, and we aim to present it in a later paper in this series; this theory has not yet given us satisfactory agreement with experiment.

10. Crystallization of the ion pools

A two-dimensional classical fluid formed from particles that interact through a repulsive Coulomb potential is expected to form a crystal with a triangular lattice when the ratio of the Coulomb potential energy in the system to the thermal energy exceeds a critical value (Crandall & Williams 1971). This ratio is conventionally represented by the parameter Γ, given by

$$\Gamma = n_0^{\frac{1}{2}} e^2 / 4\pi^{\frac{1}{2}} \epsilon_0 k_B T. \tag{10.1}$$

If the melting transition is a Kosterlitz-Thouless (1973) transition, taking place as the result of the unbinding of dislocation pairs, the critical value, Γ_c, is about 130 (Morf 1979). The transition may occur in two steps, involving an intermediate hexatic phase (Nelson & Halperin 1979). The transition to a crystalline phase has

been observed in the two-dimensional electron fluid trapped above the surface of superfluid helium (Grimes & Adams 1979), the observed value of Γ_c being 131 ± 7 (Grimes 1981), and evidence for the two-stage process has been obtained by Murray & van Winkle (1987) in experiments with colloidal suspensions of charged, 0.3 μm diameter, polystyrene–sulphonate spheres in water.

These transitions should occur in our two-dimensional ion plasmas. The fact that some motion of the ions can take place in a direction normal to the plane of the helium surface is almost certainly unimportant, since the extent of this motion is much smaller than the average spacing between the ions. For a typical ion density in our experiments (10^{11} m^{-2}) the predicted transition temperature corresponding to a value of Γ_c of 130 is 72 mK. The experiments described in this paper reveal no anomalous behaviour at this temperature; i.e. no anomalous behaviour in either the ionic effective mass or the ionic mobility, for either type of ion. We have studied pools for which the ion density has been adjusted so that the predicted transition lies within the temperature range where the mobility is phonon limited, and also so that it lies in the range where the mobility is ripplon limited, but no anomaly has been seen in either case. Nevertheless, we now know that crystallization of our pools does take place; in a very recent experiment Mellor & Vinen (1990) have studied the generation of capillary waves by ions that are forced into high frequency oscillation by an applied RF field and have shown that at certain frequencies there is constructive interference between the waves from different ions due to crystal formation when Γ exceeds the critical value of 130. It is clear therefore that crystal formation has a negligible effect on the ionic effective masses and on their mobilities. (Strictly speaking, this conclusion needs some qualification. As was shown by Mellor & Vinen, crystallization can apparently be inhibited by a small tilt of the cryostat. We believe that such a tilt was not normally present during the measurements reported here, but we have no direct evidence that the crystal had actually formed when these measurements were made.)

In the case of electrons trapped above the surface of liquid helium crystallization has a very large effect on both the electron effective mass and the mobility (Grimes & Adams 1979; Mehrotra *et al.* 1982). In the crystal phase the plasma dispersion relation is greatly modified by electron–ripplon interactions (Fisher *et al.* 1979); for small wavevectors the modification takes the form of a substantial change in the electron effective mass, this change arising from the formation under each electron of a dimple in the surface of the helium. A similar effect should occur with the ions, but a straightforward modification of the theory of Fisher *et al.* shows that the expected change in ionic effective mass is too small to have been observed in our experiments. Whether the mobility should be changed appreciably in the ionic case raises some delicate questions, to which we shall return in a later paper when we discuss the theory of the ripplon-limited mobility.

11. Conclusions and future work

In this paper we have described in some detail our experimental procedures for the study of two-dimensional ion-plasmas trapped below the surface of superfluid helium. We have shown how the ionic mobility can be deduced from the low-frequency response of the ions at fairly high temperatures, and we have described some fairly detailed studies of plasma resonances in the system, from which we have

PHILOSOPHICAL TRANSACTIONS OF THE ROYAL SOCIETY A MATHEMATICAL, PHYSICAL & ENGINEERING SCIENCES

been able to obtain detailed information about the ionic mobilities at low temperatures and about the ionic masses. We have shown that, within our experimental errors, crystallization of the ion pool has no observable effect on the ionic effective masses or on the ionic mobility. The results of further work will be described in later papers in this series: the theory of the ionic mobility; studies of the effect of a magnetic field; and studies of nonlinear effects in the plasma resonances at large amplitudes. Much work still remains to be done: detailed study of the crystallization of the ion pools at low temperatures; further study of the ripplon-limited ionic mobilities, particularly, for example, to determine whether or not this mobility is density dependent; and a study of the effect of ^{3}He, either dissolved in the bulk ^{4}He or adsorbed at its surface.

We are grateful to Mr E. L. Parker for the construction of much of the apparatus. The work was supported by a grant from the Science and Engineering Research Council.

Appendix A. The dispersion relation for plasma waves in a two-dimensional plasma

Consider an infinite sheet of ions of uniform charge density $n_0 e$ per unit area at the surface of liquid helium, which we take to be the $z = d$ plane. Above and below this sheet are infinite electrodes at $z = 0, h$. We denote the dielectric constant of the helium by ϵ, and we assume that there is a vacuum above the liquid surface. We are interested in the time-evolution of a small perturbation, σ, in the charge density, which gives rise to a perturbation, ϕ, in the electrical potential. Because we shall need the more general result in later papers, we shall include the effect of a uniform magnetic flux density, $\boldsymbol{B}$, applied in a direction normal to the plane of the ions.

The equations that we require are Laplace's equation for the potential, the linearized equation of motion for the ions, and the linearized continuity equation

$$\nabla^2\phi = 0 \quad (\text{except at } z = d), \tag{A 1}$$

$$\partial \boldsymbol{v}/\partial t = -(e/M)\nabla_2\phi + (e/M)\,\boldsymbol{v}\times\boldsymbol{B}, \tag{A 2}$$

$$\partial\sigma/\partial t = -n_0 e\nabla_2 \boldsymbol{v}, \tag{A 3}$$

where $\boldsymbol{v}$ is the drift velocity of the ions, and ∇_2 is the two-dimensional gradient operator. The potential ϕ must satisfy the boundary conditions

$$\phi(z = 0) = 0, \tag{A 4}$$

$$\phi(z = d) = 0, \tag{A 5}$$

$$\phi(z = d-0) = \phi(z = d+0), \tag{A 6}$$

$$\epsilon[\partial\phi/\partial z]_{z=d-0} - [\partial\phi/\partial z]_{z=d+0} = \sigma/\epsilon_0. \tag{A 7}$$

A solution of Laplace's equation that is appropriate to the symmetry of our experimental cell is

$$\phi = \phi_{km} J_m(kr)\exp(\mathrm{i}m\varphi)\exp(\pm kz), \tag{A 8}$$

where J_m is the Bessel function of order m, and where the coefficient ϕ_{km} is a function of time. Substitution into the boundary conditions (A 4)–(A 7) shows that the corresponding perturbation in the charge density is given by

$$\sigma = \sigma_{km} J_m(kr)\exp(\mathrm{i}m\varphi), \tag{A 9}$$

where $$\phi_{km}\,\sigma_{km}\,F(k)/2\epsilon_0\,k \tag{A 10}$$

and $$F(k)=\frac{2\sinh(kd)\sinh\{k(h-d)\}}{\sinh(kh)+(\epsilon-1)\sinh\{k(h-d)\}\cosh(kd)}. \tag{A 11}$$

The velocity $\boldsymbol{v}$ has components v_r and v_φ, in cylindrical polar coordinates, and it is convenient to work with the combinations

$$v^{(+)}=v_r+\mathrm{i}v_\varphi, \tag{A 12}$$

and $$v^{(-)}=v_r-\mathrm{i}v_\varphi. \tag{A 13}$$

We assume tentatively that, corresponding to (A 8) and (A 9), $v^{(+)}$ and $v^{(-)}$ have the forms

$$v^{(+)}=v^{(+)}_{km}\,J_{m+1}(kr)\exp(\mathrm{i}m\varphi), \tag{A 14}$$

and $$v^{(-)}=v^{(-)}_{km}\,J_{m-1}(kr)\exp(\mathrm{i}m\varphi). \tag{A 15}$$

Substituting these velocities into the equations of motion (A 2), and using (A 10), we find

$$\dot v^{(+)}_{km}=(eF(k)/2\epsilon_0 M)\,\sigma_{km}-\mathrm{i}\omega_c\,v^{(+)}_{km}, \tag{A 16}$$

$$\dot v^{(-)}_{km}=-(eF(k)/2\epsilon_0 M)\,\sigma_{km}+\mathrm{i}\omega_c\,v^{(-)}_{km}, \tag{A 17}$$

where $\omega_c=eB/M$. Rewriting the continuity equation (A 3) in terms of the velocities $v^{(+)}$ and $v^{(-)}$, we find

$$\dot\sigma=-(\tfrac{1}{2}n_0\,e)\{v^{(+)}_{km}-v^{(-)}_{km}\}\exp(\mathrm{i}m\varphi)\,J_m(kr); \tag{A 18}$$

i.e. $$\dot\sigma_{km}=-(\tfrac{1}{2}n_0\,e)\{v^{(+)}_{km}-v^{(-)}_{km}\}. \tag{A 19}$$

Eliminating σ_{km} between (A 16), (A 17) and (A 19), we obtain

$$\ddot v^{(+)}_{km}+\mathrm{i}\omega_c\,\dot v^{(+)}_{km}+\beta(k)\,v^{(+)}_{km}-\beta(k)\,v^{(-)}_{km}=0, \tag{A 20}$$

and $$\ddot v^{(-)}_{km}-\mathrm{i}\omega_c\,\dot v^{(-)}_{km}+\beta(k)^{(-)}_{km}-\beta(k)\,v^{(+)}_{km}=0, \tag{A 21}$$

where $\beta(k)=n_0\,e^2F(k)/4\epsilon_0 M$. From equations (A 20) and (A 21) we find that the coefficients $v^{(+)}_{km}$, etc., oscillate with time with angular frequency given by

$$\omega^2=\omega_c^2+2\beta(k). \tag{A 22}$$

This confirms that (A 8), (A 9), (A 14) and (A 15) represent a normal mode of oscillation of the system, with the dispersion relation (A 22). The boundary condition $v_r=0$ at $r=R$ leads to the values of k that are allowed by the condition

$$(\omega-\omega_c)\,mJ_m(kR)-\omega kRJ_{m+1}(kR)=0 \tag{A 23}$$

Appendix B. Numerical simulation of the ion pool

(a) *Introduction*

In this appendix we outline the various numerical calculations that we have carried out on the behaviour of the ion pool. We describe first the procedure used to determine the density profile of the pool in its approach to static equilibrium; then the calculation of the charge induced by the ion pool on the upper electrodes; and finally the method used to calculate the capacitances, C_i, introduced in §5. Our analysis neglects the finite electric susceptibility of the helium: the necessary corrections can be applied, but the errors resulting from their neglect are small.

The relevant dimensions of the cylindrical box containing the ion pool were defined in figure 1. For the simulation the surface at $z = d$ is divided into concentric rings. We define the ring i as that area of width $\Delta = a/N$ between an outer radius $r_i = i\Delta\,(i = 1, \ldots, N)$ and an inner radius r_{i-1}. For clarity we shall use the notation $[x] = n\pi x/h$ in the equations that follow.

To simulate the behaviour of the ion pool we need to find the total radial component, E, of the electric field that exists at the outer boundary of each ring, at $r = r_i$ and $z = d$. This field is composed of a component due to the voltages applied to the electrodes and another due to the ion pool itself. To allow the ion pool simulation to run at a reasonable rate, computations are made at the outset of the fields E due to the application in turn of unit potential to each electrode and unit charge density to each ring. These values are then stored and can be used to determine straightforwardly the electric fields due to any initial ion-density profile with any voltages applied to the electrodes.

(*b*) *Contribution of the electrode voltages to the radial electric field*

Expressions for the radial component, E, of the electric field at the radius r_i due to unit potentials on the various electrodes can be obtained from formulae quoted by Jackson (1975) and are as follows.

$$\frac{E_i^{(1)}}{V^{(1)}} = \frac{2}{h}\sum_{n=1}^{\infty}\sin[d]\frac{I_1[r_i]}{I_0[a]}, \tag{B 1}$$

$$\frac{E_i^{(2)}}{V^{(2)}} = -\frac{2}{h}\sum_{n=1}^{\infty}\frac{\{1-(-1)^n\}}{I_0[a]}\sin[d]\,I_1(r_i), \tag{B 2}$$

$$\frac{E_i^{(4)}}{V^{(4)}} = \frac{2}{a^2}\sum_{n=1}^{\infty}G(k_n)\,J_1(k_n r_i), \tag{B 3}$$

where

$$G(k_n) = \frac{\{aJ_1(k_n a) - bJ_1(k_n b)\}\sinh(k_n d)}{\sinh(k_n h)\,J_1^2(k_n a)} \tag{B 4}$$

and the k_ns are the roots of the equation

$$J_0(k_n a) = 0. \tag{B 5}$$

The superscripts (1), (2) and (4) refer to electrodes H1, H2, and H4 (figure 1). J_0 and J_1 are Bessel functions and I_0 and I_1 are modified Bessel functions.

(*c*) *Contribution of the charge in the pool itself to the radial electric field*

Consider a ring of charge within the pool, the ring having radius r, infinitesimal width $\mathrm{d}r'$, and uniform charge density σ'. As is easily shown from formulae given by Jackson (1975) this ring gives rise to a contribution to the electrostatic potential at radius r in the plane at height z that is given by

$$\phi = \frac{2\pi r'\sigma'\,\mathrm{d}r'}{\pi\epsilon_0 h}\sum_{n=1}^{\infty}\sin[d]\sin[z]\frac{I_0[r_<]}{I_0[a]}\{I_0[a]K_0[r_>] - K_0[a]I_0[r_>]\}, \tag{B 6}$$

where I_0 and K_0 are modified Bessel functions, and $r_<$ ($r_>$) are the smaller (larger) of r and r'. It is assumed that all electrodes are held at zero potential. In the present calculation we are interested in the potential in the plane of the ions, so we put $z = d$.

We next calculate the electric field at radius r_i due to the ring of charge between r_j and r_{j-1} (the jth ring) by differentiating ϕ with respect to r and then integrating with respect to r' between the limits r_{j-1} to r_j. If the jth ring lies outside the ith ring we find

$$E_i^{(j,\,\mathrm{out})} = -\frac{2\sigma_j}{\epsilon_0 h}\sum_{n=1}^{\infty}\sin^2[d]\frac{I_1[r_i]}{I_0[a]}\{I_0[a](r_{j-1}K_1[r_{j-1}]-r_jK_1[r_j]) - K_0[a](r_jI_1[r_j]-r_{j-1}I_1[r_{j-1}])\}, \quad \text{(B 7)}$$

if it lies inside we find

$$E_i^{(j,\,\mathrm{in})} = \frac{2\sigma_j}{\epsilon_0 h}\sum_{n=1}^{\infty}\sin^2[d]\frac{\{I_0[a]K_1[r_i]+K_0[a]I_1[r_i]\}}{I_0[a]}\{r_jI_1[r_j]-r_{j-1}I_1[r_{j-1}]\}, \quad \text{(B 8)}$$

where we have assumed that the charge density in the jth is constant and equal to σ_j. These formulae fail (lead to divergences) if the radius r_i adjoins the jth ring. We avoid this divergence as follows. If $j = i$ we replace r_j by $(r_j - \Delta/10)$ in the expression for $E_i^{(j,\,\mathrm{in})}$; if $j = i+1$ we replace r_{j-1} by $r_i + \Delta/10$ in the expression for $E_i^{(j,\,\mathrm{out})}$; and we assume that the 'missing charge' between radii $r_i - \Delta/10$ and $r_i + \Delta/10$ gives rise to a field at radius r_i given by

$$E_i^{(\mathrm{self})} = \frac{2\hat{\sigma}_i}{\epsilon_0 h}\sum_{n=1}^{\infty}\sin^2[d]\left\{\frac{r_1I_1[r_i]}{I_0[a]}(I_0[a]K_1[r_1]+K_0[a]I_1[r_1]) - \frac{r_2I_1[r_2]}{I_0[a]}(I_0[a]K_1[r_i]+K_0[a]I_1[r_i])\right\}, \quad \text{(B 9)}$$

where $r_1 = r_i + \Delta/10$ and $r_2 = r_i - \Delta/10$. The uniform charge density $\hat{\sigma}$ is obtained by uniformly distributing the missing charge over the region between radii $r_i - \Delta/10$ and $r_i + \Delta/10$.

(*d*) *The dynamics of the pool and its equilibrium configuration*

By summing the fields calculated in (*c*) over all the rings of width Δ in the pool, and adding the fields calculated in (*b*) due to the electrodes, we find the total electric field E_i experienced by ions at the outer boundary (radius r_i) of the ith ring. Using the equation of motion (3.1) of the ions we can calculate the rate of transfer of charge across this outer boundary. The discrete form of the equation of motion is

$$\partial v_i/\partial t = (e/M)E_i + F_i, \quad \text{(B 10)}$$

where v_i is the ionic drift velocity at the radius r_i, and

$$F_i = -v_i(e/M\mu) - v_i(v_{i+1}-v_{i-1})/2\Delta. \quad \text{(B 11)}$$

Suppose now that the charge densities σ_i and velocities v_i are known to have the values $\sigma_i^{(n)}$ and $v_i^{(n)}$ at time t_0. At time $t_{n+1} = t_n + \delta t$, where δt is a suitable time-step, the velocity v_i will have changed to

$$v_i^{(n+1)} = v_i^{(n)} + \int_{t_n}^{t_{n+1}} \mathrm{d}t\,[(e/M)E_i + F_i]. \quad \text{(B 12)}$$

This equation is solved by an iterative procedure. It is assumed that during the time interval between t_n and t_{n+1} the field E_i can be taken as a quadratic function of $(t-t_n)$, the coefficients being determined by the values of E_i at time steps t_n, t_{n-1} and

t_{n-2}, while the value of F_i can be taken as the average of its values at t_{n+1} and t_n. The fact that E_i is reasonably accurately represented enables us to cope with a field that oscillates rapidly in time, such as that present during a forced plasma resonance; for the purposes of our simulation it is not necessary to represent F_i so accurately.

Given the values of $v_i^{(n)}$ at the various time intervals t_n we can determine the rate at which charge is transferred from one ring to another (we use an integral version of the continuity equation (3.2) to ensure conservation of charge), and hence we can find the values of $\sigma_i^{(n)}$ for successive values of n. In other words we can find the way in which the charge distribution in the pool evolves in time. If the potentials applied to the electrodes are steady, then the pool settles down after a time of order $M\mu/e$ to an equilibrium state, from which we can determine equilibrium charge distributions of the type illustrated in figure 4. Our studies of the way in which the charge distribution approaches equilibrium has enabled us to demonstrate that the boundary condition for plasma resonances in our pools is that the edge of the pool remains approximately fixed, as described in §7.

(*e*) *Charge induced by the ion pool in the top electrodes*

As we explained in §§2 and 3, we complete a set of measurements on a given ion pool by measuring the charge induced in the electrodes H3 and H4 by the ion pool. We now explain how to relate this induced charge to the total charge in the pool. With a knowledge of this total charge and of the electrode potentials we can use the results of the simulations described in the earlier parts of this appendix to determine the radius and charge density of the pool.

To obtain the induced charge density at any point on the upper electrodes we need to calculate the electric field just below that point generated by the charge in the ion pool. To facilitate the necessary numerical computation we divide the top electrode system (at $z = h$) into N concentric rings, exactly as we did at the surface of the liquid (at $z = d$) in our earlier calculations. We note in passing that, besides calculating the charge induced by the ion pool, we can also calculate that induced by the potentials on the other electrodes, from which we can obtain the interelectrode capacitances. We do not give the details of these latter calculations here, but we have carried them out and checked that the resulting capacitances agree with experiment. This check serves to verify the validity of our numerical methods.

The potential at height z and radius r due to an infinitesimally thin ring of charge in the pool has already been written down as equation (B 6) (electrodes at zero potential). The corresponding electric field just below the top electrodes has only a z component, which is obtained by differentiating (B 6) with respect to z and then putting $z = h$. Formulae, analogous to (B 7) and (B 8), can then be obtained for the z-component of the electric field at radius r_i just below the top electrodes due to the charge density σ_j in the jth ring of thickness Δ in the pool.

The values of the electric field at the different radii r_i enable us to calculate the induced charge density on the upper electrodes at these radii. The charge density at other radii is obtained by linear interpolation. Integration of this charge density over the area of the top electrodes (excluding the small area of insulator separating electrodes H3 and H4) gives the required total induced charge in terms of the pool radius and the ion density.

(f) Calculation of the C_i

These effective capacitances were defined in §5. As a first step in calculating them we compute by the method outlined in (b), (c) and (d) of this Appendix, the quantity

$$\Delta\sigma(r) = \sigma'(r) - \sigma(r), \tag{B 13}$$

where $\sigma(r)$ is the equilibrium charge distribution for the particular pool of interest, when the upper electrodes, H3 and H4, are grounded, and $\sigma'(r)$ is the equilibrium charge distribution for the same pool when the electrode H4 is held at potential V_4. We then analyse $\Delta\sigma(r)$ in terms of the Bessel functions that correspond to the spatial forms of the axisymmetric resonant modes of the pool; i.e.

$$\Delta\sigma(r) = \sum_{n=1}^{\infty} a_n J_0(\lambda_n r) = \sum_{n=1}^{\infty} \sigma_n(r), \tag{B 14}$$

where the $\lambda_n R$ is the nth root of $J_1(\lambda_n R) = 0$, and R is the radius of the pool with density profile $\sigma(r)$. We have assumed that the boundary condition for the plasma resonant modes is that the edge of the pool remains fixed, as it does, to a good approximation, when the potential V_4 is applied.

As in (c) of this Appendix, we consider the potential at radius r and height z due to a ring of charge $2\pi\sigma(r')\,r'\,\mathrm{d}r'$ in the plane of the pool. This potential is given by (B 6), or, more conveniently for our present purpose, by the equivalent formula (Jackson 1975)

$$\phi = \frac{2\pi r'\sigma'\,\mathrm{d}r'}{\pi\epsilon_0 a} \sum_{n=1}^{\infty} \frac{J_0(k_n r)\,J_0(k_n r')\sinh(k_n d')\sinh\{k_n(h-z)\}}{k_n a J_1^2(k_n a)\sinh(k_n h)}, \tag{B 15}$$

where $k_n a$ is the nth root of $J(ka) = 0$; it is assumed that $z > d$, and that all the electrodes are held at zero potential. It follows that the potential due to the mth normal mode in the decomposition (B 14) of $\Delta\sigma$ is given by

$$\phi^{(m)} = \frac{2Ra_m J_0(\lambda_m R)}{\epsilon_0 a^2} \sum_{n=1}^{\infty} \frac{J_1(k_n R)\,J_0(k_n r)\sinh(k_n d)\sinh(k_n(h-z))}{J_1^2(k_n a)\sinh(k_n h)\{k_n^2 - \lambda_m^2\}}. \tag{B 16}$$

From this potential we can calculate the electric field just below the top electrodes, and hence the charge density induced on these electrodes. Integration of this charge density over the area of electrode H3 gives the total induced charge on this electrode, which when divided by V_4 gives the required capacitance C_m.

Appendix C. Effect of tilting the cryostat on the plasma resonant frequencies

The effect on the static charge distribution in the ion pool of tilting the cryostat can be understood rather easily by using the simplified analysis presented towards the end of §3, particularly the dish-and-water model, in which we assumed for simplicity that the pool is exactly midway between the upper and lower electrodes. To a first approximation the effect will be equivalent to a tilting of the dish; the position and shape of the pool are therefore hardly altered, but a density gradient is set up across the pool. Let a point in the pool be denoted by the polar coordinates (r, φ), and suppose that the cryostat is tilted through an angle γ in the plane $\varphi = 0$.

Then we see that an originally uniform ion charge density $n_0 e$ will be perturbed so that it becomes

$$n_0 e + (4\epsilon_0/h^2)(V_4 - V_1)\gamma r \cos\varphi, \tag{C 1}$$

where $V_4 - V_1$ is the potential difference between the top and bottom electrodes. We now outline a method by which the resulting changes in the plasma resonant frequencies can be calculated. For the sake of generality, and because we shall need the results in later papers, we allow for the presence of a uniform vertical magnetic field, as in Appendix A.

The potential, ϕ, associated with any perturbed plasma resonant mode of angular frequency ω can be written

$$\phi = \sum_{k_i,\, m} \phi_{km} J_m(k_i r) \exp(\mathrm{i}m\varphi) \exp(-\mathrm{i}\omega t), \tag{C 2}$$

where we have used the notation of Appendix A, and where the k_is are the values of k allowed by the boundary condition at the edge of the pool (i.e. the k_is are the roots of equation (A 23)). From the potential (C 2) we derive the corresponding values of charge σ and velocity $\boldsymbol{v}$, as in Appendix A, and then substitute into the continuity equation (A 3). We multiply the resulting equation by

$$r J_{m'}(k_j) \exp(-\mathrm{i}m'\varphi),$$

and integrate over the area of the pool. The resulting set of simultaneous equations (for different m' and j) leads to a secular equation for the frequencies of the perturbed modes. We assume that the perturbation represented by equation (C 1) is small, and handle the problem by perturbation theory.

Suppose that the unperturbed state is the (0, 1) mode. We find that to first order the shift in frequency vanishes. There is, however, a shift in second order, and we find that it is given by the equation

$$\begin{aligned}\omega^2 - \omega_1^2 = &-\frac{\pi^2\alpha^2\Omega_1^2}{I_{10}\,k_1^2} \sum_{k_i,\, m=\pm 1} \frac{\Omega_i^2}{k_i^2 I_{i1}(\omega_i^2 - \omega_1^2)} \\ &\times \left[\int_0^R J_1(k_i r)\{m k_1^2 r^2 J_0(k_1 r) + k_1 r(m + \omega_c/\omega_1) J_1(k_1 r)\}\,\mathrm{d}r\right] \\ &\times \left[\int_0^R J_0(k_1 r)\{m k_i^2 r^2 J_1(k_1 r) - (1+m)(1-\omega_c/\omega_1) J_1(k_i r) \right. \\ &\left. + k_i r(1 - m\omega_c/\omega_1) J_{m+1}(k_i r)\}\,\mathrm{d}r\right],\end{aligned} \tag{C 3}$$

where ω_1 is the unshifted frequency of the (0, 1) mode in the presence of the magnetic field, Ω_{mi} is the unshifted frequency of the (m, i) mode in the absence of the magnetic field, R is the radius of the pool,

$$\alpha = (4\epsilon_0\gamma/n_0 e h^2)(V_4 - V_1), \tag{C 4}$$

and

$$I_{km} = 2\pi \int_0^R J_m^2(k_i r)\, r\,\mathrm{d}r. \tag{C 5}$$

References

Atkins, K. R. 1959 *Phys. Rev.* **116**, 1339–1343.

Barenghi, C. F., Mellor, C. J., Muirhead, C. M. & Vinen, W. F. 1986 *J. Phys.* C: *Solid State Phys.* **19**, 1135–1144.

Baym, G., Barrera, C. J. & Pethick, C. J. 1969 *Phys. Rev. Lett.* **22**, 20–23.

Careri, G. 1961 *Progress in low temperature physics* (ed. C. J. Gorter), vol. III, p. 58. Amsterdam: North-Holland.

Crandell, R. S. & Williams, R. 1971 *Phys. Lett.* **34** A, 404–405.

Dahm, A. J. & Sanders, T. M. 1970 *J. Low Temperature Phys.* **2**, 199–222.

Dahm, A. J. & Vinen, W. F. 1987 *Physics Today* **40**, 43–50.

Elser, V. & Platzman, P. M. 1988 *Phys. Rev. Lett.* **61**, 177–179.

Elser, V. & Platzman, P. M. 1990 *Phys. Rev. Lett.* **64**, 103.

Fisher, D. S., Halperin, B. I. & Platzman, P. M. 1979 *Phys. Rev. Lett.* **42**, 798–801.

Glattli, D. C., Andrei, E. Y., Deville, G., Poitrenaud, J. & Williams, F. I. B. 1985 *Phys. Rev. Lett.* **54**, 1710–1713.

Gradshteyn, I. S. & Ryzhik, I. M. 1980 *Table of integrals, series, and products* (ed. A. Jeffrey). New York: Academic Press.

Grimes, C. C. 1981 *Physica* A **106**, 102–107.

Grimes, C. A. & Adams, G. 1979 *Phys. Rev. Lett.* **42**, 795–798.

Hannahs, S. & Williams, G. A. 1987 *Jap. J. appl. Phys.* **26**, suppl. 26-3, 741–742.

Jackson, J. D. 1975 *Classical electrodynamics*. New York: Wiley.

Kosterlitz, J. M. & Thouless, D. J. 1973 *J. Phys.* C: *Solid State Phys.* **6**, 1181–1203.

Lambert, D. K. & Richards, P. L. 1981 *Phys. Rev.* B **23**, 3282–3290.

Landau, L. D. & Lifshitz, E. M. 1959 *Fluid mechanics*. London: Pergamon Press.

Mehrotra, R., Guenin, B. M. & Dahm, A. J. 1982 *Phys. Rev. Lett.* **48**, 641–644.

Mellor, C. J., Muirhead, C. M., Traverse, J. & Vinen, W. F. 1988 *J. Phys.* C: *Solid State Phys.* **21**, 325–331.

Mellor, C. J. & Vinen, W. F. 1990 *Surface Sci.* **229**, 368–370.

Morf, R. H. 1979 *Phys. Rev. Lett.* **43**, 931–935.

Murray, C. A. & van Winkle, D. H. 1987 *Phys. Rev. Lett.* **58**, 1200–1203.

Nelson, D. R. & Halperin, B. I. 1979 *Phys. Rev.* B **19**, 2457–2484.

Ott-Rowland, M. L., Kotsubo, V., Theobald, J. & Williams, G. A. 1982 *Phys. Rev. Lett.* **49**, 1708–1712.

Ott-Rowland, M. L., Kotsubo, V., Theobald, J. & Williams, G. A. 1983 *Proc. 75th Jubilee Conf. on Helium-4* (ed. J. M. G. Armitage), pp. 154–155. Singapore: World Scientific.

Poitrenaud, J. & Williams, F. I. B. 1972 *Phys. Rev. Lett.* **29**, 1230–1232. (Erratum: *Phys. Rev. Lett.* **32**, 1213 (1974).)

Prasad, S. A. & Morales, G. J. 1988 *Phys. Fluids* **30**, 3475–3484.

Putterman, S., Roberts, P. H. & Fiszdon, W. 1988 *Phys. Lett.* A **128**, 203–206.

Schoepe, W. & Rayfield, G. W. 1973 *Phys. Rev.* A **7**, 2111–2121.

Schwarz, K. W. 1972*a* *Phys. Rev.* A **6**, 837–844.

Schwarz, K. W. 1972*b* *Phys. Rev.* A **6**, 1958–1966.

Schwarz, K. W. 1975 *Adv. Chem. Phys.* **33**, 1.

Shikin, V. B. 1970 *Sov. Phys. JETP* **31**, 936–940.

Tao Pang 1988 *Phys. Rev. Lett.* **61**, 849–852.

Tao Pang 1990 *Phys. Rev. Lett.* **64**, 104.

Theobald, J., Ott-Rowland, M. L. & Williams, G. A. 1981 *Physica* B+C **108**, 957–958.

Williams, G. A. & Theobald, J. 1980 *Phys. Lett.* **77** A, 255–257.

Received 16 May 1990; accepted 22 June 1990

PHILOSOPHICAL TRANSACTIONS OF THE ROYAL SOCIETY A MATHEMATICAL, PHYSICAL & ENGINEERING SCIENCES